SCIENTIFIC REPORTS

OPEN

SUBJECT AREAS:
CANCER MODELS
TRANSLATIONAL RESEARCH
SEMICONDUCTOR LASERS
BIOPHOTONICS

Received
20 February 2013

Accepted
25 November 2013

Published
12 December 2013

Correspondence and requests for materials should be addressed to S.G.S. (s.sokolovski@dundee.ac.uk)

Infrared laser pulse triggers increased singlet oxygen production in tumour cells

S. G. Sokolovski[1], S. A. Zolotovskaya[1], A. Goltsov[2], C. Pourreyron[3], A. P. South[3] & E. U. Rafailov[1]

[1]Photonics and Nanoscience Group, School of Engineering, Physics and Mathematics, University of Dundee, Dundee DD1 4HN, UK, [2]Centre for Research in Informatics and Systems Pathology (CRISP), University of Abertay Dundee, DD1 1HG, UK, [3]Division of Cancer Research, Medical Research Institute, Ninewells Hospital and Medical School, University of Dundee, Dundee, DD1 9SY, UK.

Photodynamic therapy (PDT) is a technique developed to treat the ever-increasing global incidence of cancer. This technique utilises singlet oxygen ($^1O_2$) generation via a laser excited photosensitiser (PS) to kill cancer cells. However, prolonged sensitivity to intensive light (6–8 weeks for lung cancer), relatively low tissue penetration by activating light (630 nm up to 4 mm), and the cost of PS administration can limit progressive PDT applications. The development of quantum-dot laser diodes emitting in the highest absorption region (1268 nm) of triplet oxygen ($^3O_2$) presents the possibility of inducing apoptosis in tumour cells through direct $^3O_2 \rightarrow {}^1O_2$ transition. Here we demonstrate that a single laser pulse triggers dose-dependent $^1O_2$ generation in both normal keratinocytes and tumour cells and show that tumour cells yield the highest $^1O_2$ far beyond the initial laser pulse exposure. Our modelling and experimental results support the development of direct infrared (IR) laser-induced tumour treatment as a promising approach in tumour PDT.

The application of laser technology to diagnostic and therapeutic regimens across different medical fields has become widespread, encompassing diverse specialities ranging from ophthalmology to oncology. Since Diamond et al. in 1972 first successfully killed glioma cells in culture and in gliomas subcutaneously transplanted in rats with haematoporphyrin and visible light exposure photodynamic therapy has been used for the treatment of various cancers. The technique is based on the photodynamic effect (PDE) inducing damage (DNA, membranes, etc.) in a photosensitised cell in the presence of light and oxygen[1–3]. Briefly, photodynamic therapy uses a selectively localised light-sensitive drug (PS) that can absorb light and directly generate radicals (type I reaction) and activating molecular oxygen (type II reaction) to produce reactive oxygen species (ROS) in sufficient quantity to kill tumour cells. However, the PS is absorbed both by healthy tissues and by the tumour leading to in some cases prolong sensitivity of patients to intensive light. Due to this side effect, and the low tissue penetration by activating light (630 nm, up to 4 mm[4–6]), the low specificity of PSs to cancer types, and the cost of PS administration (for oesophageal carcinoma with post PDT period of 4–6 days £4370–6000)[7], there is a need for further research in PDT methods. Therefore there is strong interest in the development of cancer phototherapy without the need for a PS[8]. Recent development of quantum-dot (QD) laser diodes (LDs) emitting in the near infrared (NIR) spectral range offers such an opportunity to develop direct laser therapy of cancer. The QD-LD emission wavelength centred at around 1268 nm coincides well with the near IR absorption band[9] of oxygen molecule[10]. One particular opportunity involves activation of the apoptotic response through direct molecular oxygen photoexcitation. To date the idea of $^1O_2$ activation has not attracted much attention because direct $^3O_2 \rightarrow {}^1O_2$ transition in molecular oxygen is prohibited on the basis of spin-orbital selection rules. However new experimental development in solvent effect on the spin forbidden transitions of molecular oxygen have redrawn the selection rules governing the intermolecular enhancement[11,12]. The enhancement of $^3O_2 \rightarrow {}^1O_2$ transition has been attributed to the major intensity contribution from O_2-O_2 bi-molecular collisions, which mix electron orbital states by an intermolecular exchange interaction, introducing some allowed characters into previously forbidden transitions. Furthermore, the action spectra in the range from 310 to 860 nm demonstrated for low-intensity laser therapy in a number of cell cultures[13] suggest that transformation of cell metabolism in response to low power laser is consistent with absorption bands of molecular oxygen. $^1O_2$ formation by direct photoexcitation with 1265 nm in pigment-free aerobic systems[14] and in condensed phase at 77 K with 1064 nm[15] have also been demonstrated. Recently it was shown that 1270 nm laser could induce cancer cell death in PS-free medium[16]. This pioneering research by Anquez et al. has clearly demonstrated cancer cells growth suppression induced by extensive 1270 nm laser irradiation[16]. However, direct monitoring of ROS (e.g., $^1O_2$ or O^-_2) in the cell and cellular mechanisms of this laser effect remain unclear[16]. Therefore, we aimed to study whether 1268 nm

irradiation by quantum dot laser can directly transform triplet oxygen to its active form singlet O_2 in organic solution and in different cell lines without PSs also modelling laser-induced oxidative stress mechanisms and addressing the question whether this light wavelength exposure can kill cancer cells. To dissect the cellular mechanism of direct ROS generation by 1268 nm laser irradiation we developed a kinetic model of a redox homeostasis alteration and oxidative stress under pulse laser exposure. The main aim of the modelling is to elucidate a liminal nature of laser-induced oxidative stress followed by apoptosis signal[17]. As it has been shown in the modelling of radiation-induced oxidative stress in bacterium[18], the threshold effect can be due to antioxidant cellular system and oxidative stress is reached when this protective system becomes saturated and overwhelmed under irradiation. To consider this mechanism in the model we took into account the laser-induced perturbation of the protective antioxidant cellular system which is assumed to be overwhelmed in cancer cells due to a constant endogenous oxidative stress[19]. Given these conditions we show by computational simulation that at PS-free medium laser irradiation is capable of triggering prolonged cellular oxidative stress (accumulation of ROS) by the impulse perturbation of redox homeostasis in cancer cells.

Results

Singlet oxygen photo-generation in organic solution in the present of molecular oxygen. To investigate the direct photo-activation of molecular oxygen we used a well-known scavenger of singlet oxygen (naphthacene in carbon tetrachloride) as a substrate for the photo-oxygenation assessments[20]. The solvent concentration was 200 μM so that the solvent quenching was low and the singlet oxygen quenching would be the dominant process[7]. The difference in absorption at a given wavelength before and after laser irradiation was used as a measure of the $^1O_2$ formation ratio. The interaction of naphthacene in carbon tetrachloride with $^1O_2$ is known to be purely chemical, accompanied by formation of endoperoxides and loss of absorbance in the visible spectral range. The absorption spectrum of naphthacene shows no resolvable absorption at 1268 nm (Fig. 1A, insert) negating the possibility that the laser pulse can directly bleach naphthacene. The 20-min 1268 nm irradiation led to appreciable bleaching of the air-saturated solutions with a twofold increase in the bleaching rate in oxygen-purified solutions at an irradiation dose of 1200 J/cm^2. Control 830 nm LD pulse induced no detectable changes (within a measurement error of 2%) of naphthacene absorption even in oxygen-enriched solutions. The absorption spectra of a control sample before and after 830-nm laser irradiation and a negative control as a measure of photobleaching under normal room lighting conditions are shown in Fig. 1A. Oxidation of naphthacene was determined by the $^1O_2$ generation after direct 1268 nm laser $^3O_2$ photoexcitation suggesting that similar photo-oxidation reactions might be detected in living cellular systems.

Laser-induced $^1O_2$ production in living cells. The feasibility of oxygen photo-activation in the absence of PSs in true living cell systems remains uncertain. However the results of low-intensity laser therapy[21], modification of red blood cell membrane proteins[22], and cancer cell growth suppression in PS free-conditions[16] by photo-excitation in the near infrared spectral range suggests that direct photo-oxidation in media containing molecular oxygen is apparent. Since the feasibility of oxygen photo-activation in the absence of PSs in true bio-systems is still unclear we chose dihydroethidium (DHE), which is specifically oxidized to dihydroxyethidium (DHOE) fluorescing at 585 nm[23] by the superoxide anion (O_2^-, the first by-product of $^1O_2$ reduction[10] and ROS precursor in the cell[23]), to monitor singlet oxygen in immortalised epidermal keratinocytes (HaCaT)[24] before, during, and after laser pulse irradiation. Experiments using HaCaT cells showed a significant difference between non-irradiated cells and those irradiated by a 1268 nm laser pulse of 47.7 J/cm^2 causing an increase in DHOE (oxidized DHE) fluorescence with a lag-phase of 40–60 seconds reaching a steady-state level after 8 min and continued post termination of the laser pulse (Fig. 1B–D). At the same time, a strong donor of O_2^- NaOCl (100 μM) induced a dramatic increase in DHOE fluorescence. The pre-incubation of HaCaT cells for 10 min with α-tocopherol (a nonspecific ROS scavenger[25,26]) diminished the laser-induced fluorescence to near background levels. This suggests that the 1268 nm laser irradiation photo-oxidizes molecular oxygen inside the cell.

Next, we investigated primary keratinocytes (PK) and HeLa cells. As shown in figure 1C the 1268 nm laser pulse triggered O_2^--dependent fluorescence in all three cell types with the most dramatic effect observed in HeLa cells and no difference between HaCaT and PK. The near IR laser-induced fluorescence demonstrated strong dose dependency without reaching saturation for the time, especially in HeLa cells (Fig. 1D). The increased sensitivity of HeLa cells could be explained by their malignant origin resulting in a high metabolic state leading to a weaker free radical defence system[19] compared with noncancerous cells[27]. A LD emitting at 830 nm was employed as a temperature control as nearly identical heating was evident compared with 1268 nm LD. The 830 nm irradiation (119.4 J/cm^2) having no absorption by O_2 shows no effect on O_2^--dependent fluorescence in any cell types (Fig. 1D) underpins the hypothesis that only irradiation absorbed by oxygen (1268 nm, etc.) can induce ROS production through singlet oxygen photoactivation. This observation together with temperature control experiments (Fig. 1D and S2, Supplementary Info) rules out suggestion that 1268 nm laser can generate extensive heat which induces significant amount of $^1O_2$ in the cell. Most intriguing was the observation of a continued increase in ROS level inside the cells even after the laser had ceased, most prominent in HeLa cancer cells.

Cytosolic free calcium level and ion channel activity under laser pulses. Products of oxidative stress (ROS, NO, organic radicals, etc.) are recognized as powerful regulatory messengers in cell signalling which very often affect cell calcium homeostasis[28]. In turn calcium homeostasis disruption can contribute to oxidative stress[29]. From our results, we anticipated that laser-induced $^1O_2$ production could reflect on cytosolic calcium concentration ($[Ca^{2+}]_{cyt}$). Therefore single cell ratiometric Ca^{2+} imaging was employed to estimate calcium response of the HaCaT and HeLa cell lines after 1268 nm irradiation of 47.7 J/cm^2 (Fig. 2A). Imaging showed an apparent increase in the fluorescence ratio by more than 1.2 times for HaCaT and HeLa cells, registered immediately after the laser was on. Following the cessation of irradiation, $[Ca^{2+}]_{cyt}$ was measured for at least 7 min and found to continue rising in HaCaT cells whilst in contrast to the laser-induced singlet oxygen response, HeLa cells demonstrated plateau (discussed below). Further application of NaOCl (100 μM) induced a typical oxidative-stress-like calcium response in all cell lines (Fig. 2A). The LD emitting at 830 nm also temporally increased calcium fluorescence in both cell types falling to basic levels after the pulse was terminated.

To answer where IR irradiation-induced calcium originates from external or internal calcium stores we monitored single channel activities (Fig. 2B, traces) on the plasma membrane of HaCaT cells with a patch clamp in a cell-attached configuration before (I), during (II) and after (III) an IR pulse. The analysis of single-channel activity demonstrated a typical pattern (current amplitude 5–25 pA and dwell open time around 1–3 ms) associated with non-excited low-voltage activated Ca^{2+} channels[30]. The significant increase in channel activity by more than an order of magnitude was observed at the end of laser pulse (3 min) indicating that plasma membrane Ca^{2+} channels were activated by ROS-induced calcium release from internal stores (Fig. 2A; 2B, III). Pre-incubation with α–tocopherol (10 μM) for 10 minutes decreased general channel activity and fully prevented

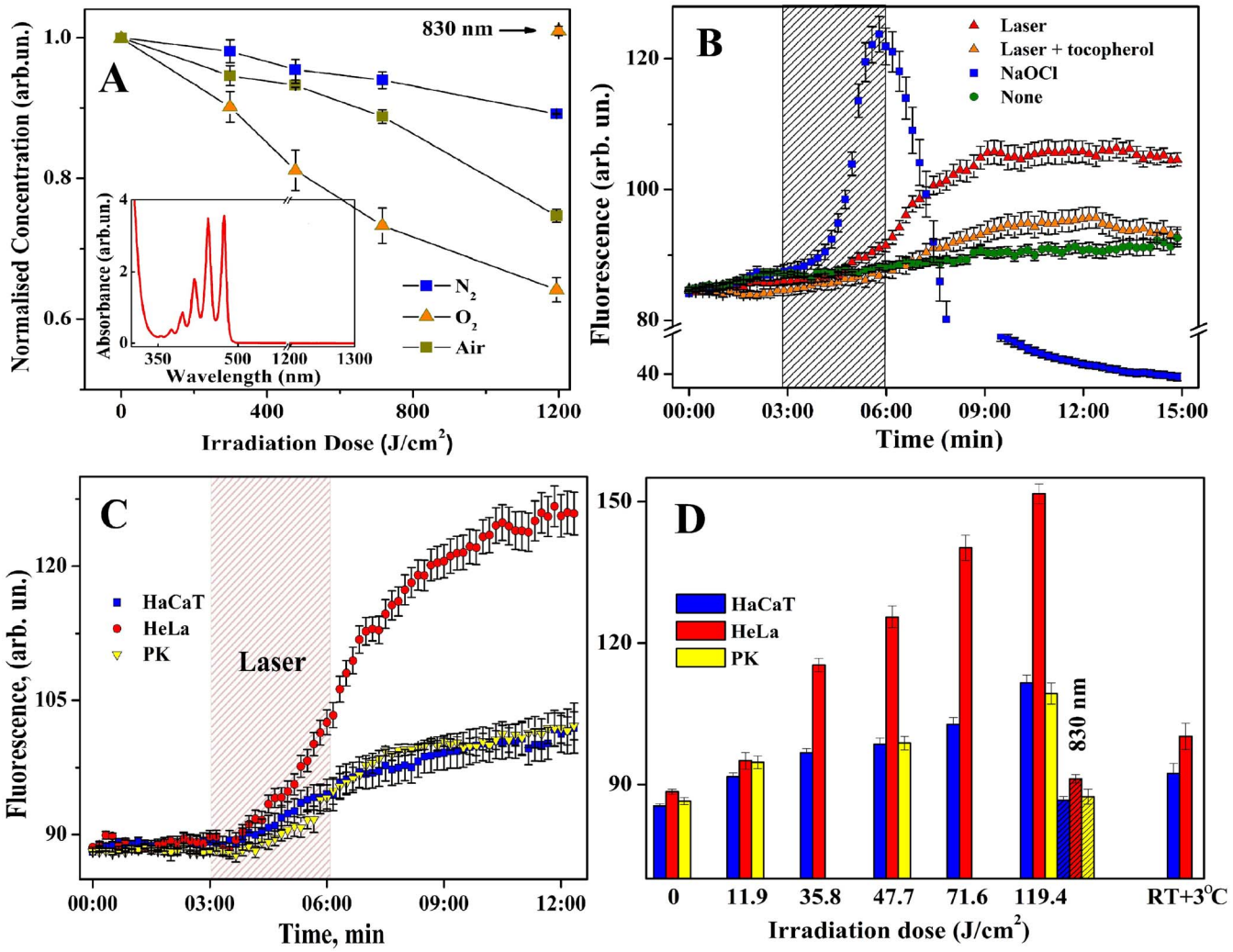

Figure 1 | Laser-induced singlet oxygen generation in CCl_4 and different cell lines. (A) Naphthacene photobleaching in oxygen-, air-, and nitrogen-saturated CCl_4. (n = 3, mean ± SD). *Insert*: Absorption spectrum of naphthacene. (B) Effect of 1268 nm irradiation of 47.7 J/cm² along on DHOE fluorescence in HaCaT cells, and with 10 μM α-tocopherol, or 100 μM NaOCl only, background fluorescence (none). Means of n = 3, 20–30 cells per each ± SE. (C) Kinetics of laser-induced DHOE fluorescence in HaCaT, HeLa cells, and primary keratinocytes and (D) dose-dependency of DHOE fluorescence in all deferent cell lines taken at 12th min of recording. 830 nm laser irradiation (slash line pattern) taken as a negative control. Mean of n = 5 (20–30 cells per each) ± SE.

IR-induced channel activation (Fig. S1) pointing to ROS as the initial origin of the laser effect on channel activity.

Modelling laser-induced oxidative stress in the cell. For comprehensive analysis of our results, a kinetic model of redox homeostasis and its imbalance by laser-induced ROS generation in normal and cancerous cells was developed (Fig. 3 and 4A).

The model reproduces a low basal level of primary ROS, H_2O_2, and secondary oxygen radicals in the absence of laser irradiation, up to 3 min before laser impulse (Fig. 4A, green, red, and black plots respectively). The model results mimic experimental data of H_2O_2 low concentration (0.01 μM[4]) in normal functioning cells. Such low level of ROS in the model is achieved due to the ROS scavenging processes considered (see Methods).

In the model, a 3 minute laser pulse (Fig. 3B, blue dashed line) caused the generation of $^1O_2$ (the precursor of various ROS). As the lifetime of $^1O_2$ is short in the cell (~5 μs[31]), it quickly decays through oxidation of cellular species and formation of radicals, in particular O_2^{-}[10]. O_2^- dismutates into H_2O_2 being a source of secondary oxygen radicals as a result of Fenton reactions[32]. The model predicts a rapid growth of H_2O_2 after the laser is applied and an immediate stop after the laser is removed (Fig. 3B, red line). Such H_2O_2 accumulation has been observed in water during exposure to 1264 nm laser irradiation[33]. To model the ideal conditions of H_2O_2 scavenging we introduced the enzymatic antioxidant system (including Px, PSH, Red, see Methods) which causes the fall of H_2O_2 concentration to basal levels during 5 min after the laser is removed. Due to scavenging of excessive H_2O_2 the concentration of both reduced enzymes of antioxidant system decrease from steady state concentrations by factor ten (Fig. 3B, blue and dashed black lines). During this time, H_2O_2 generates a secondary oxygen radical pool, R_2 (Fig. 3B, black line). To estimate the kinetic parameters of the model (Table S1 and S2), the total kinetics of primary and secondary radicals generated by laser pulse was fitted against the experimental data on radicals generated by different laser irradiation doses V_{laser} in HaCaT cells (Fig. 4A).

To simulate laser-induced ROS production in cancer cells we changed some parameters taking into account certain features of malignancy such as an initially high primary ROS production rate, V_o[4,34–36]; increased concentration of endogenous H_2O_2 and key antioxidant enzymes such as thioredoxin[37] (Trx), thioredoxin reductase (TR) by up to 6.5 times[34,37–39] and thioredoxin peroxidase (Tpx) up to 9 times[38] due to high cytosolic expression of these enzymes in cancer

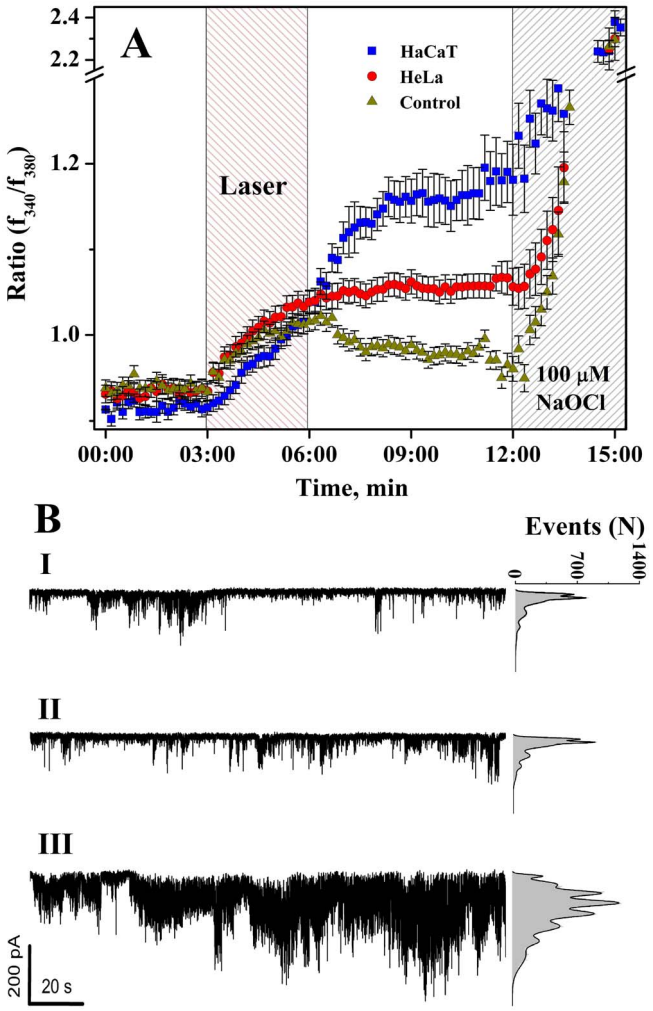

Figure 2 | Effect of irradiations on (A) calcium ratio in HaCaT (1268 nm), HeLa (1268 nm) cells, and both cell lines with 830 nm (control). Mean of n = 4, 10–15 cells per each ± SE; (B) Single channel currents recorded at −100 mV holding voltage at cell-attached configuration before (I), during (II), and after (III) 1268 nm laser irradiation of 47.7 J/cm^2. (6 cells). *Right-hand segment*: opened channel events point-amplitude.

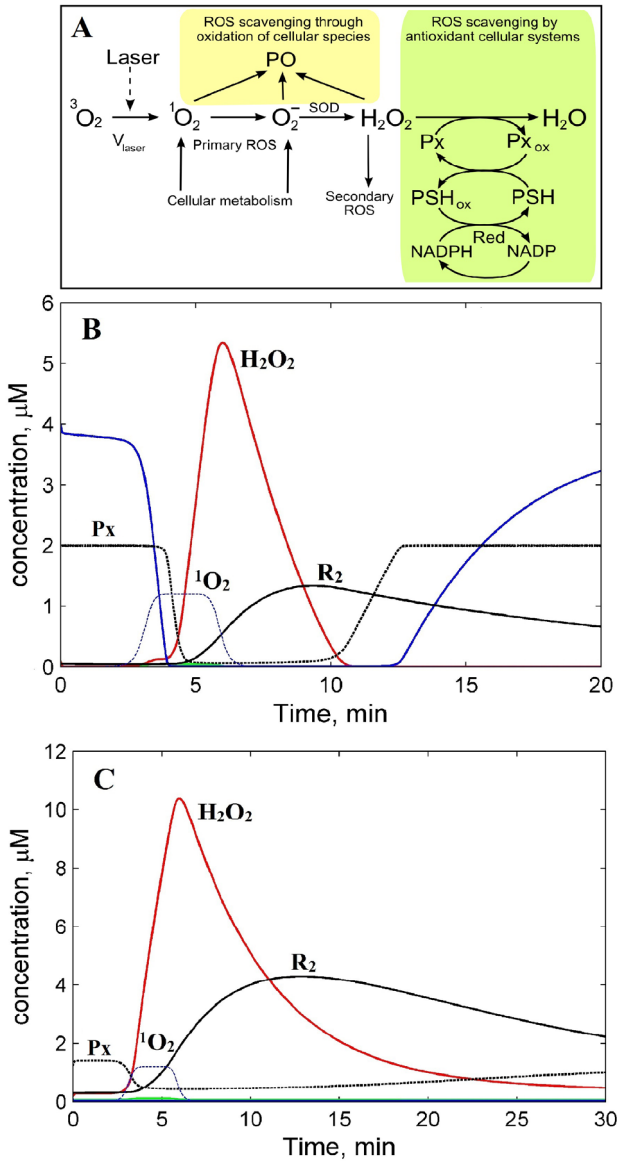

Figure 3 | **A model of cell redox homeostasis and its imbalance by laser-induced ROS generation.** (A) Scheme of cellular ROS production and scavenging. (B) Kinetics of ROS in normal and (C) cancerous cells. H_2O_2 (—); reduced PSH (—); primary ROS ($^1O_2$ and O_2^-), R_1, (—); reduced thioredoxin peroxidase, Px (- -); sum of primary and secondary ROS, R_2 (—); rate of $^1O_2$ generation by 3 min laser pulse only (- -).

cells. The best fitting of the theoretical ROS kinetics against HeLa cancer cell experimental data was obtained at 2-fold for Px, PSH and 4-fold for reductase (Red) concentrations, and H_2O_2 production rate V_o up to 7 μM/min[4]. Other model parameters were left unchanged (Fig. 4A and Tables S1 and S2).

Laser-triggered cancer cell death. To provide evidence that the 1268 nm laser can trigger apoptosis in the cell[40] we carried out a preliminary experiment to assay cell death which suggested that 1268 nm laser irradiation of 47.7 and 119.4 J/cm^2 is capable of killing HeLa cancer cells (Fig. 4B). The possibility of laser induced death as a result of cell overheating was ruled out due to temperature control experiments for cell death ($\Delta t \leq 6$–7.5°C) measurements (Fig. 4B). The fact that 47.7 J/cm^2 (200 mW) laser dose caused higher HeLa cell death rate than 119.4 J/cm^2 irradiation dose (Fig. 4B) could be due to faster depletion of triplet oxygen in the cells during higher power 500 mW (119.4 J/cm^2) laser pulse. These data and Anquez et al. results point to the fact that prolonged but low power 1268 nm laser irradiation is preferable for effective cancer cell killing rather than short-pulsed but powerful laser treatment.

Discussion

Soon after its inception nearly forty years ago, photodynamic therapy became popular as a promising approach to cure malignant tumours[8]. However, clinical practice revealed significant limitations in the use of this method mainly due to the post-treatment hypersensitivity of patients to intensive light and the low depth of tissue penetration by active light irradiation at 630 nm. The idea of direct phototransformation of triplet to singlet O_2 with 1270 nm laser irradiation originated from the observed absorption spectrum previously thought to be spin-forbidden[11] and readily used to detect singlet O_2 forms of luminescence at this wavelength[15]. This was originally shown in pigment-free aerobic systems[14], protein and cell suspensions[22]. However these data were generated using irradiation doses which exceed safety margins for cancer therapy. Our experiments in anoxia solution with a wider range of irradiation doses starting from 240 J/cm^2 clearly demonstrated that QD LD emitting around 1268 nm can directly generate singlet oxygen in CCl_4

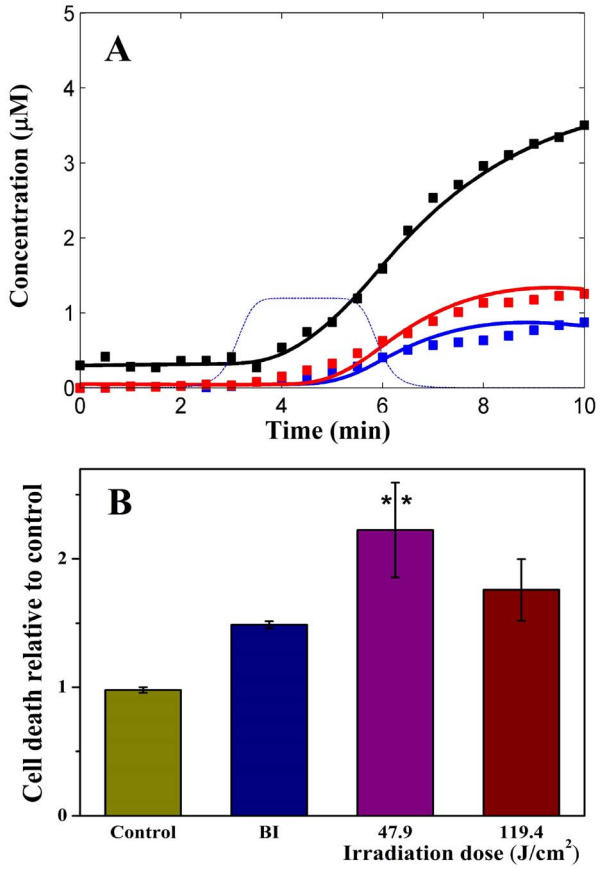

Figure 4 | Kinetics of ROS production in noncancerous cells at the different rates of singlet oxygen generation (A): $V_{laser,1}$ (−) and $V_{laser,2} > V_{laser,1}$ (−) and in cancer cells at $V_{laser,1}$ (−). Laser-induced singlet oxygen production rate used for modelling (---). Experimental data of ROS production at 47.7 J/cm² (■) and 71.6 J/cm² (■) in HaCaT and 47.7 J/cm² in HeLa (■) cells; and (B) HeLa cell death rate measured by an enzymatic assay of LDH release. BI 2536 (a PLK1 inhibitor) was used as a positive control. Graph shows a mean ± SE of one experiment, (n = 3).

solution only in the presence of molecular oxygen (Fig. 1A). This led us to suppose that, once triggered by the laser, singlet oxygen might then lead to further ROS production within the cell, which could potentially trigger apoptosis in cancer cells without the need for PSs[14].

Indeed HaCaT cells loaded with DHE demonstrated after 3 min that a 1268 nm laser pulse increased DHOE fluorescence in the cytoplasm (Fig. 1B). The fact that the laser pulse transited $^3O_2$ to $^1O_2$ only in O_2 containing solution (Fig. 1A) and that α-tocopherol abolished the laser-induced DHOE fluorescence in the cell, identifies singlet O_2 as the origin of the effects and demonstrates for the first time this mechanism in a true cellular system (Fig. 1B). Most intriguing is the observation that cancer cells (HeLa) demonstrate hypersensitivity to 1268 nm LD irradiation compared with normal keratinocytes (Fig. 1C, D). These data also suggest that 1268 nm LD can be used to directly photoactivate molecular oxygen *in vivo*. Furthermore, the dosage of radiation based on the kinetics model data (see Fig. 3 and 4A) could be selected to strike a balance between therapeutic efficacy and undesirable damage to cells. The observation that laser-induced $^1O_2$ generation shows significant delay in reaching steady-state levels of ROS after laser cessation prompted the idea that the laser excitation overcame the cellular ROS defence system particularly in the cancer cells[34,41].

It is common knowledge that apoptosis can be triggered by many different stimuli, including cytokines, oxidative stress, and calcium release from the endoplasmic reticulum. Calcium release from the ER synchronizes the massive leak of cytochrome *c* from the mitochondria orchestrating apoptosis[34,42]. Oxidative stress itself can lead to massive disturbance of cell calcium homeostasis[43] and *contra versa*[44] demonstrating in some cases a tight ROS-Ca^{2+} feedback loop[28]. The significantly higher $[Ca^{2+}]_{cyt}$ response to 1268 nm LD irradiation observed in HaCaT cells compared with HeLa cells (Fig. 2A) can be attributed to a general high reactivity of keratinocytes to ROS described in[45]. These results suggest that the observed increase in $[Ca^{2+}]_{cyt}$, Ca^{2+} channel activity and $^1O_2$-production in the cell is likely to be associated with direct molecular oxygen photoactivation by 1268 nm irradiation. Cancerous HeLa cells have a higher general metabolic activity and demonstrate the highest $^1O_2$ production in response to the laser pulse compared to non-cancerous cells which have a much weaker calcium response postulated as a means of protection[46,47]. Significant but reversible calcium response of both cell lines to control irradiation of 830 nm could be through activation of cytochrome *c* oxidase which can weakly absorb in the IR bandwidth leading to ROS-induced leak of calcium to the cytoplasm from mitochondria[48] which is shortly terminated in both cancer and normal cells.

The high complexity of regulation within the redox system prompted us to create a kinetics model of cell redox homeostasis and its imbalance caused by the laser to explain our experimental results. First of all the results of modelling laser-induced ROS kinetics determined significant differences between normal and cancer cells (Fig. 3BC and 4A). An initial high rate of ROS production in cancer cells determines a higher background level of H_2O_2 and oxygen radicals (both around 0.2 μM) compared with normal cells 0.01 μM (Fig. 3BC, red and black plots). However H_2O_2 concentration is still under the threshold value of 1 μM after which apoptosis can trigger[4]. Secondly, the steady state concentration of reduced enzymes of antioxidant system, Px (Tpx and Trx) and PSH (Gpx and glutathione (GSH)) calculated in the model for cancer cells is low (0.02 μM) because the scavenging system is thought to be depleted by a higher rate of H_2O_2 production due to excessive metabolism. At the same rate of laser-induced generation of $^1O_2$ ($V_{laser,o}$) in both cell types, the depletion of ROS scavenging enzymes in the cytosol of cancer cells assumes to disrupt the antioxidant system bringing the H_2O_2 concentration up to 10.5 μM which is two-fold higher than its level in normal cells (Fig. 3BC; red plots). Additionally this leads to a longer time for restoration of background concentration of H_2O_2, reductase Px, and oxygen radicals (R_2) in cancer cells after the laser is switched off (Figs. 3BC; red, dashed black, and solid black lines). The computational modelling suggests that the prolonged O_2^- generation after the initial laser pulse is determined by the size of the secondary pool of ROS generated through excessive H_2O_2 produced from the initial laser-generated $^1O_2$ (Fig. 3B). Prolonged retention of a high level of H_2O_2 results in depletion of the ROS scavenging enzyme systems followed by a slow restoration after laser irradiation (Fig. 3BC). The model thus reproduces the following features of the laser-generated oxygen radicals observed in the experiments. Firstly, the model closely describes the experimental delay of radical generation observed at the start of laser pulse (Fig. 3C). The delay obtained in the model happens due to deferred generation of secondary radicals which significantly contribute to the total ROS levels comparing with fast laser-triggered primary radicals (Fig. 3B, black and green plots respectively). A bare contribution of primary radicals ($^1O_2$ and O_2^-) to the total ROS yield comes in part from fast conversion of $^1O_2$ to O_2^- that dismutates to longer living H_2O_2. Secondly, the model reproduces the experimental observations that ROS production lasts longer beyond the laser pulse (Fig. 1B, C, and 3B, C). Such a significant level of H_2O_2 shown by the model after laser irradiation is a result of slower degradation due to a depletion of the ROS scavenging system (level of the reduced antioxidant enzymes, Px and PSH) and high H_2O_2 concentrations (Fig. 3B, red line). The model shows that

ROS concentrations gradually decrease after 10 min because of the restoration of the scavenging system (an increase in Px and PSH) (Fig. 3B, blue and black dashed lines). Full restoration of ROS and the scavenging system to background levels perturbed by laser irradiation is predicted to be 30 min after laser irradiation is stopped.

To model the relatively high ROS generated in the cancer cells (Fig. 1C, D) we have changed the model parameters to consider a higher rate of general ROS production (V_o) and higher expression of the main antioxidant enzymes[37,38] in cancer cells. The ROS kinetics computed with these parameters closely mimicked a high ROS accumulation in cancer compared with noncancerous cells (Fig. 4A, black plot) which is in agreement with our experimental data (Fig. 1C–D). We conclude that the higher laser-induced ROS levels observed in cancer cells might result from the depletion in cellular scavenging systems caused by a high general ROS production (Fig. 3BC) involving calcium homeostasis disruption and could be a trigger for apoptosis in cancer cells. Additional laser multi-impulse experiments for further model development will be needed to find optimal laser pulse frequency, duration and power for effective induction of oxidative stress in cancer cells leaving normal cells unharmed.

Finally, our experimental and computational results explaining high ROS levels in cancer cells together with the fact that 1268 nm laser can induce cytotoxicity in HeLa cells may in near future propose a new therapeutic approach based on direct laser photoactivation of molecular oxygen in the tumour without the need for exogenous drugs gain opportunity to develop PS-free cancer phototherapy.

Methods

Laser characteristics. A fibre coupled InGaAs/InAs quantum dot laser diodes (Innolume GmbH) in continuous wave regime were used as an irradiation sources. They have an emission spectrum centred at 1268 and 830 nm.

Measuring of singlet oxygen in organic solution. $^1O_2$ levels in carbon tetrachloride (Fluka) were measured as described in[20] with the naphthacene (Sigma-Aldrich) with PerkinElmer Lambda-900 UV/VIS/NIR spectrometer. A control sample (3 ml) was photo-bleached under normal room lighting. Dose dependent $^1O_2$ formation ratio was measured after 20 min at atmospheric pressure and room temperature (23°C, RT).

Cell lines culture. Cell lines were cultivated as described in[27] and[49]. Prior to all experiments the confluent cells were disaggregated with a 0.1% tyrosine/EDTA for 3–10 min, transfer to modified phosphate-free Tyrode's medium (TM) (in mM: 140 NaCl, 3.6 KCl, 1.2 $MgCl_2$, 1.8 $CaCl_2$, and 10 HEPES, pH 7.4) and kept on ice. Prior to fluorescence and patch clamp experiments cells were placed for 20 min to medium perfused chamber (1 ml/min) where the temperature did not exceed RT by more than 3°C during LD pulse with highest power of 500 mW. The temperature in the perfused chamber and during following cancer cell death assay experiments was monitored under laser beam with TC-8 thermocouple Data Logger and PicoLog software (Pico Technology, USA).

Monitoring $^1O_2$ level and $[Ca^{2+}]_{cyt}$ in single cell. $^1O_2$ measurements in HaCaT, HeLa, and PK with DHE[23] (5 μM, Invitrogen) were conducted with fluorescent microscope Axio Obersver A1 accomplished with AxoCam MRm camera and AxioVision 4.8.1 software (Zeiss). Fluorescence from cell nucleus area were acquired and normalized to background cell fluorescence before LD pulse.

Imaging of cytoplasm free calcium in HaCaT and HeLa was performed as described in_[50] on the same microscope with fluorescent filter set (340 nm and 380 nm). Fura-2 (Molecular Probes) fluorescence from cell cytoplasm was acquired and fluorescence ratio was calculated with AxioVision software.

Single channel patch clamp recording. Single channel recordings of HaCaT cells were made with Axopatch 200B amplifier at cell-attached configuration with TM in pipette/chamber with holding potential of −100 mV. Data acquisition and single channel analysis were made with pCLAMP10.0 (Molecular Devices).

Cell death rate assay. Death rate assay of HeLa cells was performed 24 hours after treatments (irradiation, temperature control, and BI2536 application) using the CytoTox 96® Non-Radioactive Cytotoxicity Assay (Promega) according to the manufacturer's instructions. This assay measures lactate dehydrogenase (LDH) activity in extracellular medium when this enzyme is released upon cell lysis. Cells were seeded at high density in 12-well plates at 0.5×10^6/well in DMEM supplemented with 10% FBS. The following day, media were changed for 0.5 ml of raw DMEM at room temperature (RT, 21°C for 119.4 J/cm^2 and 23°C for 47.9 J/cm^2) and cells were irradiated 3 min with 1268 nm laser either 47.9 J/cm^2 or 119.4 J/cm^2 doses. Temperature controls corresponding to the variation in temperature over RT due to irradiation ($\Delta t = 6$°C for 47.9 J/cm^2 and 7.5°C for 119.4 J/cm^2) were made by heating cells for 3 min in a water bath set to 29.3°C for 47.9 J/cm^2 and 28.5°C for 119.4 J/cm^2. The highest temperature reached during irradiation was 29.3°C. Raw DMEM was changed for DMEM supplemented with 10% FBS after irradiation and the cells were placed back in incubators. A positive control of cell death was performed by treating cells for 24 hours with 5 μM PLK1 inhibitor BI2536.

Computational method. A scheme of the model is given in Fig. 3A. The model takes into account the following processes: (i) endogenous generation of primary ROS (O_2^-, $^1O_2$) and laser-produced $^1O_2$, denoted by the variable R_1; (ii) their transformation into H_2O_2 by superoxide dismutase (SOD); (iii) generation of a secondary pool of ROS from H_2O_2 through the Fenton reactions (R_2); and (iv) scavenging H_2O_2 and its by-products by the cellular antioxidant system. Considering that the cellular antioxidant system involves many enzymes utilising H_2O_2 we phenomenologically modelled this system. The enzymatic sub-model of the H_2O_2 degradation is based on the redox cascade reactions which correspond to the key antioxidant cellular systems: thioredoxin peroxidase/thioredoxin/thioredoxin reductase (Tpx/Trx/TR) and glutathione peroxidase/glutathione/glutathione reductase (Gpx/GSS/GR) systems[32]. This sub-model is represented in Fig. 3A by the reactions and enzymes which we denoted by Px (peroxidases Tpx and Gpx degrading H_2O_2), PSH (GSH and Trx, protein containing thiol groups), and Red (reductases TR and GR redusing GSS and Trx). Note, in the model we did not consider genetic feedback regulation of the antioxidant enzyme expression induced by oxidative stress through activation of different signalling pathways such as NF-κB, Nrf2, HIF, and others[17]. However, we took into account an increase in the expression level of the antioxidant proteins (Px and PSH) in cancer cells in comparison with normal ones[34,37–39].

The model was calibrated based on both the experimental data on kinetic parameters available from literature and our experimental kinetics data on ROS generation by laser at two irradiation doses in HaCaT and HeLa cells. Detailed description of the model and a set of model parameters obtained are given in *Supplementary Information*. The total concentration of primary R_1 and secondary R_2 radicals generated by laser irradiation was the readout of the model which is compared with experimental radical kinetics in our experiment. This phenomenological model was used to describe laser-induced change in cellular redox homeostasis leading to depletion of enzymatic antioxidant system and ROS accumulation in cells.

1. Harrod-Kim, P. Tumor ablation with photodynamic therapy: Introduction to mechanism and clinical applications. *J. Vascul and Interven Radiol* **17**, 1441–1448 (2006).
2. He, P. J. *et al.* Enhanced apoptotic effect of combined modality of 9-hydroxypheophorbide alpha-mediated photodynamic therapy and carboplatin on AMC-HN-3 human head and neck cancer cells. *Oncol Rep* **21**, 329–334 (2009).
3. Bulina, M. E. *et al.* A genetically encoded photosensitizer. *Nat Biotech* **24**, 95–99 (2006).
4. Lee, L. K., Whitehurst, C., Pantelides, M. L. & Moore, J. V. In situ comparison of 665 nm and 633 nm wavelength light penetration in the human prostate gland. *Photochem and Photobiol* **62**, 882–886 (1995).
5. Muller, P. J. & Wilson, B. C. An update on the penetration depth of 630 nm light in normal and malignant human brain tissue in vivo. *Phys in Med and Biol* **31**, 1295 (1986).
6. Stolik, S., Delgado, J. A., Pérez, A. & Anasagasti, L. Measurement of the penetration depths of red and near infrared light in human "ex vivo" tissues. *J. Photochem and Photobiol B: Biol* **57**, 90–93 (2000).
7. Matheson, I. B. C. & Lee, J. Reaction of chemical acceptors with singlet oxygen produced by direct laser excitation. *Chem Phys Lett* **7**, 475–476 (1970).
8. Diamond, I. *et al.* Photodymanic therapy of malignant tumors. *Lancet* **2**, 1175–& (1972).
9. Zakharov, S. D. & Ivanov, A. V. Light-oxygen effect in cells and its potential applications in tumour therapy. *Quant Elect* **29**, 1031–1053 (1999).
10. Halliwell, B. & Gutteridge, G. M. *Free radicals in biology and medicine* (Oxford University Press, 2007).
11. Long, C. & Kearns, D. R. Selection rules for the intermolecular enhancement of spin forbidden transitions in molecular oxygen. *J. Chem. Phys.* **59**, 5729–5736 (1973).
12. Matheson, I. B. C. & Lee, J. Comparison of the pressure dependences of the visible and infrared electronic absorption spectra of oxygen in gas and in Freon solution. *Chem. Phys. Lett.* **8**, 173–176 (1971).
13. Pavel, S. Light therapy (with UVA-1) for SLE patients: is it a good or bad idea? *Rheumatol* **45**, 653–655 (2006).
14. Krasnovsky, A. A., Drozdova, N. N., Ivanov, A. V. & Ambartsumian, R. V. Activation of Molecular Oxygen by Infrared Laser Radiation in Pigment-Free Aerobic Systems. *Biochem (Moscow)* **68**, 963–966 (2003).
15. Jockusch, S. *et al.* Singlet molecular oxygen by direct excitation. *Photochem. Photobiol. Sci.* **7**, 235–239 (2008).
16. Anquez, F. *et al.* Cancerous Cell Death from Sensitizer Free Photoactivation of Singlet Oxygen. *Photochem and Photobiol* **88**, 167–174 (2012).
17. Trachootham, D. *et al.* Redox Regulation of Cell Survival. *Antiox & Redox Sign* **10**, 1343–1374 (2008).

18. Shuryak, I. & Brenner, D. J. A model of interactions between radiation-induced oxidative stress, protein and DNA damage in Deinococcus radiodurans. *J Theor Biol* **261**, 305–317 (2009).
19. Trachootham, D., Alexandre, J. & Huang, P. Targeting cancer cells by ROS-mediated mechanisms: a radical therapeutic approach? *Nat Rev Drug Discov* **8**, 579–591 (2009).
20. Bjarneson, D. W. & Petersen, N. O. The photochemistry of naphthacene in solution. *J. Photochem and Photobiol A: Chem* **63**, 327–335 (1992).
21. Waynant, R. W. *Lasers in medicine.* (CRC Press, 2002).
22. Zakharov, S. D. *et al.* Structural rearrangements in the aqueous phase of cell suspensions and protein solutions induced by a light-oxygen effect. *Quant Elect* **33**, 149–162 (2003).
23. Peshavariya, H. M., Dusting, G. J. & Selemidis, S. Analysis of dihydroethidium fluorescence for the detection of intracellular and extracellular superoxide produced by NADPH oxidase. *Free Rad Res* **41**, 699–712 (2007).
24. Adams, J. C. & Watt, F. M. An unusual strain of human keratinocytes which do not stratify or undergo terminal differentiation in culture. *J. Cell Biol* **107**, 1927–1938 (1988).
25. Leo, S., Szabadkai, G. & Rizzuto, R. The Mitochondrial Antioxidants MitoE(2) and MitoQ(10) Increase Mitochondrial Ca2+ Load upon Cell Stimulation by Inhibiting Ca2+ Efflux from the Organelle. *Mitoch and Oxid Stress in Neurodegen Disord* **1147**, 264–274 (2008).
26. De Luca, C., Deeva, I., Mikhal'chik, E. & Korkina, L. Beneficial effects of pro-/antioxidant-based nutraceuticals in the skin rejuvenation techniques. *Cell and Mol Biol* **53**, 94–101 (2007).
27. Shim, J.-H. *et al.* E7-expressing HaCaT keratinocyte cells are resistant to oxidative stress-induced cell death via the induction of catalase. *Proteomics* **5**, 2112–2122 (2005).
28. Singh, D. K. *et al.* The Strength of Receptor Signaling Is Centrally Controlled through a Cooperative Loop between Ca2+ and an Oxidant Signal. *Cell* **121**, 281–293 (2005).
29. Brookes, P. S., Yoon, Y., Robotham, J. L., Anders, M. W. & Sheu, Sh.-Sh. Calcium, ATP, and ROS: a mitochondrial love-hate triangle. *Am. J. Physiol - Cell Physiol* **287**, C817–C833 (2004).
30. Kostyuk, P. G. Low-voltage activated calcium channels: achievements and problems. *Neurosci* **92**, 1157–1163 (1999).
31. Baier, J. *et al.* Direct Detection of Singlet Oxygen Generated by UVA Irradiation in Human Cells and Skin. *J. Invest Dermatol* **127**, 1498–1506 (2007).
32. Valko, M. *et al.* Free radicals and antioxidants in normal physiological functions and human disease. *Intl J. Biochem & Cell Biol* **39**, 44–84 (2007).
33. Gudkov, S. V. *et al.* Oxygen-Dependent Auto-Oscillations of Water Luminescence Triggered by the 1264 nm Radiation. *J. Phys Chem B* **115**, 7693–7698 (2011).
34. Schumacker, P. T. Reactive oxygen species in cancer cells: Live by the sword, die by the sword. *Cancer Cell* **10**, 175–176 (2006).
35. Luo, J., Solimini, N. L. & Elledge, S. J. Principles of Cancer Therapy: Oncogene and Non-oncogene Addiction. *Cell* **136**, 823–837 (2009).
36. Szatrowski, T. P. & Nathan, C. F. Production of Large Amounts of Hydrogen Peroxide by Human Tumor Cells. *Cancer Res* **51**, 794–798 (1991).
37. Biaglow, J. E. & Miller, R. A. The thioredoxin reductase/thioredoxin system - Novel redox targets for cancer therapy. *Cancer Biol & Therapy* **4**, 6–13 (2005).
38. Cha, M.-K., Suh, K.-H. & Kim, I.-H. Overexpression of peroxiredoxin I and thioredoxin1 in human breast carcinoma. *J. Exp. & Clinic Cancer Res* **28**, 93–95 (2009).
39. Chockalingam, K. *et al.* Engineering and characterization of human manganese superoxide dismutase mutants with high activity and low product inhibition. *FEBS J.* **273**, 4853–4861 (2006).
40. Ghavami, S. *et al.* Mechanism of apoptosis induced by S100A8/A9 in colon cancer cell lines: the role of ROS and the effect of metal ions. *J. Leukocyte Biol* **76**, 169–175 (2004).
41. Nordberg, J. & Arnér, E. S. J. Reactive oxygen species, antioxidants, and the mammalian thioredoxin system. *Free Radic Biol and Med* **31**, 1287–1312 (2001).
42. Mattson, M. P. & Chan, S. L. Calcium orchestrates apoptosis. *Nat Cell Biol* **5**, 1041–1043 (2003).
43. Rosenstock, T. R. *et al.* Mitochondrial calcium, oxidative stress and apoptosis in a neurodegenerative disease model induced by 3-nitropropionic acid. *J. Neurochem* **88**, 1220–1228 (2004).
44. Peng, T.-I. & Jou, M.-J. Oxidative stress caused by mitochondrial calcium overload. *Ann. N-Y Acad Sci* **1201**, 183–188 (2010).
45. Hitoshi, M., Yukiko, I., Shoichi, Y. & Yuri, O. Reactive Oxygen Species in HaCaT Keratinocytes After UVB Irradiation Are Triggered by Intracellular Ca^{2+} Levels. *J. Invest Dermat Symp Proc* **14**, 50–52 (2009).
46. Marklund, S. Spectrophotometric study of spontaneous disproportionation of superoxide anion radical and sensitive direct assay for superoxide dismutase. *J. Biol Chem* **251**, 7504–7507 (1976).
47. Furuya, Y. *et al.* The Role of Calcium, pH, and Cell Proliferation in the Programmed (Apoptotic) Death of Androgen-independent Prostatic Cancer Cells Induced by Thapsigargin. *Cancer Res* **54**, 6167–6175 (1994).
48. Karu, T. I. Mitochondrial signaling in mammalian cells activated by red and near-IR radiation. *Photochem and Photobiol* **84**, 1091–1099 (2008).
49. Kovacs, D. *et al.* Keratinocyte growth factor down-regulates intracellular ROS production induced by UVB. *J. Dermatol Sci* **54**, 106–113 (2009).
50. Williams, D. A. Quantitative intracellular calcium imaging with laser-scanning confocal microscopy. *Cell Calcium* **11**, 589–597 (1990).

Acknowledgments

Authors thanks Dr P. Campbell and Prof W.H.I. McLean for laboratory support and Prof. A. Thompson for critical remarks to the manuscript and FP7 FAST-DOT and SICSA (Scottish Informatics and Computer Science Alliance), and Dr G. Malcolm from M-squared Ltd for partial financial support of this work.

Author contributions

E.U.R. initiated and supervised the project. *S.G.S.* has performed main part of fluorescence and patch clamp experiment as well as data analysis. *S.A.Z.* has carried out photochemistry experiments with naphthacene, partly involved in fluorescence experiments. *A.G.* proposed the oxidative stress kinetic model. *C.P.* and *A.S.* perform all experiments on cell death rate assay. All authors participated in discussion of the results and the manuscript writing.

Additional information

Supplementary information accompanies this paper at http://www.nature.com/scientificreports

Competing financial interests: The authors declare no competing financial interests.

How to cite this article: Sokolovski, S.G. *et al.* Infrared laser pulse triggers increased singlet oxygen production in tumour cells. *Sci. Rep.* **3**, 3484; DOI:10.1038/srep03484 (2013).